Early W and Z Measurements at ATLAS

C. Mills, for the ATLAS collaboration
Harvard University, Cambridge, MA 02138, USA

The first measurements of the W and Z cross sections in pp collisions at $\sqrt{s} = 7$ TeV using the ATLAS detector at the Large Hadron Collider (LHC) have been completed. Cross sections in the electron and muon channels , as well as the combined cross section, are presented for both the W and the Z boson. The charge asymmetry of W production as a function of the psuedorapidity of the lepton has also been measured.

1. INTRODUCTION

Observation of the W and Z bosons in $\sqrt{s} = 7$ TeV proton-proton collisions at the LHC is an important milestone in the ATLAS physics program. These are the first cross section measurements at 7 TeV that can be compared to a theoretical calculation of comparable precision. Also, they are the most common source of isolated, high transverse momentum leptons, and are therefore an important data sample for understanding final states based on leptons.

The W and Z bosons were first observed by the UA1 and UA2 experiments at CERN nearly thirty years ago, in proton-antiproton collisions at $\sqrt{s}$ =540 GeV [1–4]. Since then, their properties have been characterized in detail by a succession of collider experiments. Now, confirmation of their known properties, such as their masses and widths, and completion of collider-specific measurements, such as their inclusive and differential cross sections, are a priority in the physics program of a new collider such as the LHC.

In the analyses described here, the W decays to a charged lepton and a neutrino, and the Z decays to two charged leptons of opposite sign. The charged leptons may be either electrons or muons. The isolated, energetic leptons allow a very pure signal to be identified above the background. The observed data are compared to the signal and background expectations. The signal acceptance times efficiency is calculated from Monte Carlo simulations, with corrections for differences between real and simulated detector performance. Background expectations are also derived primarily from simulation, with some use of data to make the QCD background expectations more robust. This knowledge combined allows calculation of the production cross sections for the W and Z. Using the same information, the lepton charge asymmetry for W production is also measured.

2. THE ATLAS DETECTOR

The ATLAS detector [5] at the LHC consists of concentric cylindrical layers of inner tracking, calorimetry, and outer (or muon) tracking, with both the inner and outer tracking volumes contained in the fields of superconducting magnets to enable measurement of charged particle momenta. In the ATLAS coordinate system, the z axis points along the anti-clockwise beam direction, and the azimuthal and polar angles ϕ and η are defined in the conventional way, with $\phi = 0$ (the x axis) pointing from the origin to the center of the LHC ring. The pseudorapidity is defined as $\eta = -\ln\tan(\theta/2)$. The transverse momentum p_T, the transverse energy E_T, and the transverse missing energy $E_{\mathrm{T}}^{\mathrm{miss}}$ are defined in the $x - y$ plane.

The Inner Detector (ID) provides precision tracking of charged particles inside of $|\eta| \approx 2.5$. It is located immediately around the interaction point, inside a superconducting solenoid which produces a 2 T axial field. The innermost layers use silicon pixel and strip tracking technology, and the outer layers are a gaseous tracker which also provides transition radiation information.

The calorimeter system surrounds the ID and the solenoid. It covers the pseudorapidity range $|\eta| < 4.9$ and has a minimum depth of 22 electromagnetic radiation lengths (X_0). The liquid argon (LAr) electromagnetic (EM) calorimeter uses a lead absorber in folded layers designed to minimize gaps in coverage. The LAr calorimeter is segmented in depth to enable better particle shower reconstruction. The innermost layer, or "compartment" is

instrumented with strips that precisely measure the shower location in η. The middle compartment is the deepest and contains most of the electromagnetic shower produced by a typical electron or photon. The outermost compartment has the coarsest granularity and is used to quantify how much of the particle shower is leaking back into the hadronic calorimeter.

The outermost tracking layers, interleaved with superconducting air-core toroid magnets, form a muon spectrometer. Precision tracking in the bending plane ($R-\eta$) for both the barrel and the endcaps is done by drift tubes. In the innermost forward plane, from $2.0 < |\eta| < 2.7$, precision spacepoints are provided by cathode strip chambers. Resistive plate chambers and thin gap chambers are used in the barrel and endcap muon triggers, respectively. In addition to fast readout for triggering, these detectors provide ϕ hit information for offline muon reconstruction.

3. CANDIDATE DATA SAMPLES AND MODELING OF SIGNAL AND BACKGROUND

The W cross section and asymmetry measurements shown here use approximately 17 nb^{-1} of integrated luminosity. Electron events are selected online through a hardware-based trigger that selects events with an electromagnetic cluster with $E_T > 5$ GeV and $|\eta| < 2.5$. Muon events are selected online by comparing the pattern of hits in the muon spectrometer to a lookup table based on muon tracks. The W analysis uses a muon trigger with "open roads", that is, no explicit p_T threshold.

The Z cross section measurement uses 219–229 nb^{-1}of integrated luminosity. Because the additional data used was acquired after the data for the W analysis, higher instantaneous luminosity conditions made it necessary to raise the trigger thresholds, to 10 GeV for the electron channel and 6 GeV for the muon channel.

The signal and backgrounds are modeled using Pythia [6] Monte Carlo using MRSTLO* [7] parton distribution functions (PDF) integrated with a Geant4 [8] simulation of the ATLAS detector.

4. EVENT SELECTION

Candidate W and Z events are identified based on selection of events with at least one lepton. Additional selection uses the second lepton (neutrino or charged) and the mass of the boson to enhance the signal to background ratio.

4.1. Preselection

Electrons at ATLAS are reconstructed as a calorimeter cluster matched to an Inner Detector track, with transverse energy $E_T > 20$ GeV and $|\eta| < 2.47$, excluding the range from $1.37 < |\eta| < 1.52$. Electron selection at ATLAS has three tiers of increasing stringency: "loose", "medium", and "tight". The "loose" selection uses information from the middle compartment of the LAr calorimeter to require that the shower profile is consistent with an electron. The "medium" selection adds the requirement of a high-quality matched ID track. It also uses the fine-granularity information from the innermost calorimeter layer for additional checks of the shower shape. "Tight" electrons pass additional track quality and kinematic requirements. More detail on electron identification is available in Ref. [9]. For the event preselection, all electrons passing the "loose" selection are considered. The E_T of electron candidates satisfying the preselection criteria in events passing the 5 GeV trigger are shown in Figure 1.

Muons are reconstructed by combining an inner detector (ID) and muon spectrometer (MS) track, and must have $p_T > 15$ GeV and $|\eta| \leq 2.4$ are to pass the preselection. To reduce the background from cosmic rays, the z position where a candidate muon passes the beamline must be within 1 cm of the z of a reconstructed primary vertex. Additionally, to reduce the background from decays-in-flight, the MS track of the muon is required to have $p_T > 10$ GeV and the absolute difference between the p_T measured in the MS and the ID is required to be less than 15 GeV. The p_T of all preselected muons in events passing the "open roads" trigger are shown in Fig. 1.

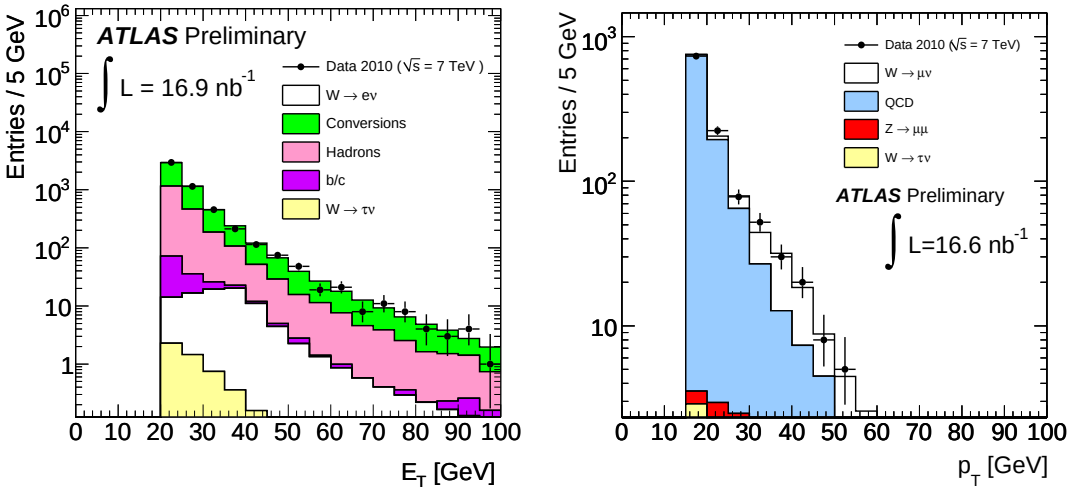

Figure 1: Transverse energy of electrons passing preselection (left) and transverse momentum of muons passing preselection (right).

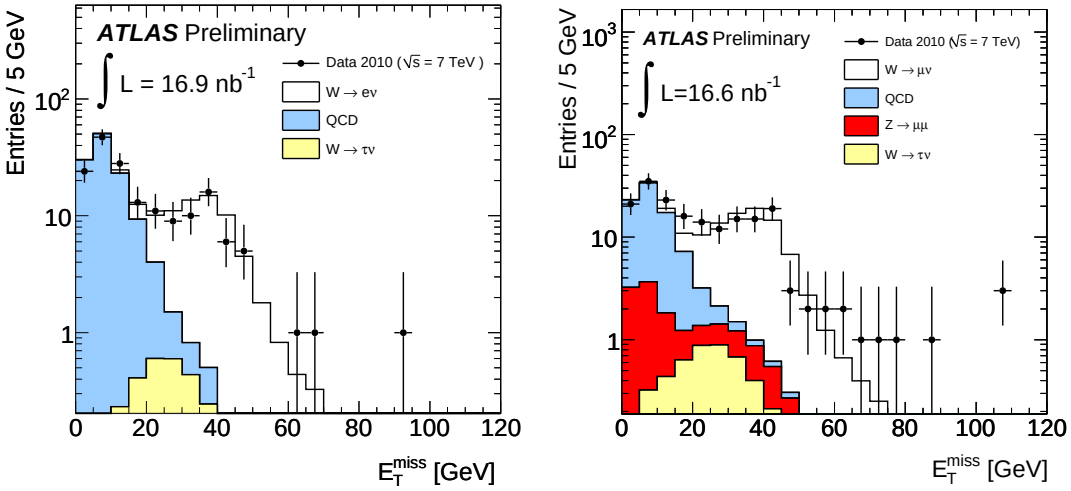

Figure 2: Missing transverse energy ($E_{\mathrm{T}}^{\mathrm{miss}}$) in events passing all lepton selection for W candidates in the electron (left) and muon (right) channels.

4.2. W Event Selection

First, extra criteria are added to the lepton selection. Electron candidates are required to pass the "tight" requirements, which have the best QCD rejection. In the muon channel, the p_T threshold is raised to 20 GeV from 15 GeV and a track isolation requirement is added to reduce backgrounds, particularly from QCD.

The missing transverse energy in $W \to \ell\nu$ events measures the transverse momentum of the neutrino produced by the W decay. The $E_{\mathrm{T}}^{\mathrm{miss}}$ in electron and muon events after the final lepton selection described in the previous paragraph is shown in Figure 2. The W event selection requires $E_{\mathrm{T}}^{\mathrm{miss}} > 25$ GeV. The transverse mass, defined as

$$M_T = \sqrt{2(p_T^{\mu})(E_{\mathrm{T}}^{\mathrm{miss}})(1 - \cos(\phi^{\mu} - \phi^{E_{\mathrm{T}}^{\mathrm{miss}}}))} \ ,$$

is a distinctive property of W events. The transverse mass distribution of candidates in the electron and muon channels after the $E_{\mathrm{T}}^{\mathrm{miss}}$ requirement is shown in Fig. 3. A requirement of $M_T > 40$ GeV completes the W event selection for both channels.

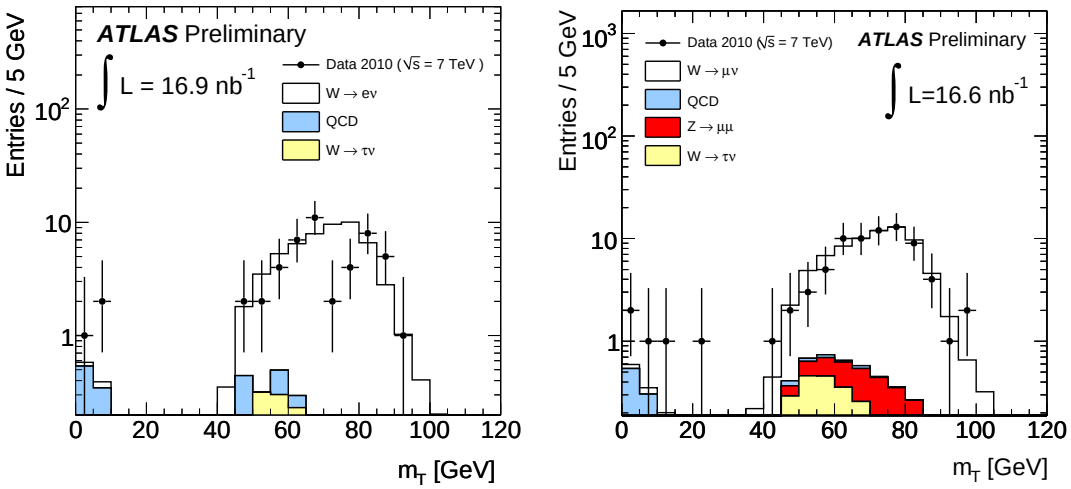

Figure 3: Transverse mass of W candidates in the electron (left) and muon (right) channels after all event selection except for the transverse mass requirement.

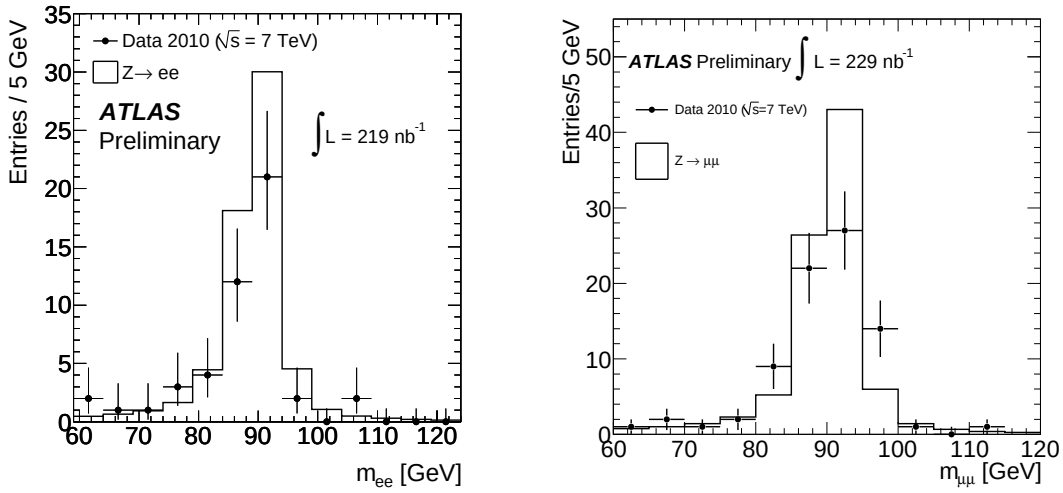

Figure 4: Transverse mass of W candidates in the electron (left) and muon (right) channels after all event selection except for the transverse mass requirement.

4.3. Z Event Selection

For both the electron and muon channels, the Z event selection requires two same-flavor oppositely charged leptons with an invariant mass reconstructed in the range $66 < M_{\ell\ell} < 116$ GeV. In the electron channel, the electron selection is as for the W analysis, except that the electrons are only required to pass the "medium" selection, increasing the acceptance. Muons are selected identically to the W analysis. The invariant mass distribution of Z candidates immediately before the $M_{\ell\ell}$ requirement is shown in Fig. 4.

5. W ACCEPTANCE AND ASSOCIATED SYSTEMATIC UNCERTAINTIES

The $W \to \ell\nu$ acceptance times efficiency can be factorized into a geometrical and kinematic acceptance A_W and a correction factor C_W for reconstruction efficiency and resolution effects. In the analysis presented here, both are

Table I: Components of the $W \to \ell\nu$ acceptance times efficiency, with associated systematic uncertainties.

channel	A_W	C_W	**acceptance x efficiency**
electrons	0.462 ± 0.014	0.656 ± 0.053	0.303 ± 0.026
muons	0.480 ± 0.014	0.814 ± 0.056	0.391 ± 0.029

Table II: Components of the $Z \to \ell\ell$ acceptance times efficiency, with associated systematic uncertainties.

channel	A_Z	C_Z	**acceptance x efficiency**
electrons	0.446 ± 0.013	0.645 ± 0.090	0.288 ± 0.091
muons	0.486 ± 0.014	0.797 ± 0.055	0.387 ± 0.057

calculated from PYTHIA, although C_W is corrected for observed discrepancies between true and simulated detector performance where possible. Table I shows A_W, C_W, and their product, the total acceptance times efficiency, for both the electron and muon channels.

The acceptance A_W is defined as the fraction of all generated events passing the following criteria at truth level: $p_T^\ell > 20$ GeV, $p_T^\nu > 25$ GeV, $M_T > 40$ GeV, as well as $|\eta_e| < 1.37$ or $1.52 < |\eta_e| < 2.47$ or $|\eta_\mu| < 2.4$. The systematic uncertainty on the acceptance A_W, 3%, is common between the electron and muon channels. The dominant contribution is from differences between the PYTHIA acceptance calculation and the acceptance as calculated using the MC@NLO [10] generator. The uncertainty also includes the differences observed in the acceptance when the PDF set used is varied.

The correction factor C_W is the ratio of the number of events passing all of the $W \to \ell\nu$ event selection after full reconstruction to the number of events passing the truth-level selection. The systematic uncertainty on C_W includes the uncertainties on the trigger and reconstruction efficiencies, as well as the uncertainty on the lepton and $E_{\mathrm{T}}^{\mathrm{miss}}$ energy scale and resolutions. The total is 8% for the electron channel and 7% for the muon channel.

6. Z ACCEPTANCE AND ASSOCIATED SYSTEMATIC UNCERTAINTIES

The $Z \to \ell\ell$ acceptance times efficiency is similarly factorized into a geometrical and kinematic component A_Z and a correction for detection efficiency C_Z. These components, and their product, the total acceptance times efficiency, are shown together with their associated uncertainties in Table II.

The geometrical and kinematic acceptance A_Z is the fraction of all generated events with $66 < m_{\ell\ell} < 116$ GeV which have two leptons with $p_T > 20$ GeV and $|\eta_e| < 1.37$ or $1.52 < |\eta_e| < 2.47$ or $|\eta_\mu| < 2.4$. The 3% systematic uncertainty on A_Z consists of approximately equal contributions from PDF uncertainties and LO-NLO differences. The efficiency correction factor C_Z is the ratio of the number of events passing all of the Z event selection to the number passing the truth-level selection described above. Because there are two charged leptons in the final state, the systematic uncertainty on C_Z is dominated by uncertainties on lepton trigger and reconstruction efficiencies in both channels. In the electron channel, the total uncertainty is 14%, and for muons, it is 7%.

7. BACKGROUND CALCULATIONS

7.1. Backgrounds to $W \to \ell\nu$

For the $W \to \ell\nu$ analyses, the $Z/\gamma^* \to \ell\ell$ and $W \to \tau\nu$ backgrounds are estimated using acceptances calculated from PYTHIA Monte Carlo simulations. The systematic uncertainties on these backgrounds are calculated similarly to the systematic uncertainties on the W acceptance times efficiency.

Table III: Results for the W cross section times branching ratio to leptons, with inputs.

channel	**int. lum. ($\mathbf{nb^{-1}}$)**	N_{cand}	$N_{\text{background}}$	**acceptance x efficiency**	$\sigma\times$ **BR (nb)**
electron	16.9	46	2.6 ± 0.5	0.303 ± 0.026	8.5 ± 1.3 (stat) ± 0.7 (sys) ± 0.9 (lum)
muon	16.6	72	5.3 ± 0.7	0.391 ± 0.029	10.3 ± 1.3 (stat) ± 0.8 (sys) ± 1.1 (lum)
combined	-	118	-	-	9.3 ± 0.9 (stat) ± 0.6 (sys) ± 1.0 (lum)

In the electron channel, the QCD background is calculated from a fit of the isolation distribution of candidate events selected using "loose" instead of "tight" electrons with $W \to e\nu$ and QCD templates from simulation. The number of QCD events resulting from the fit is scaled by a rejection factor, measured in simulation, for the tight selection relative to the loose selection. In the muon channel, the number of isolated, low-$E_{\text{T}}^{\text{miss}}$ QCD events is extrapolated to the number of isolated, high-$E_{\text{T}}^{\text{miss}}$ QCD events by multiplying it by the ratio of the number of non-isolated, high-$E_{\text{T}}^{\text{miss}}$ events to the number of non-isolated, low-$E_{\text{T}}^{\text{miss}}$ events. The uncertainties on both QCD background estimates contain a significant statistical contribution. The systematic uncertainties on the QCD backgrounds are based on variations of the methods used for the electron channel and the results of a closure test in simulation for the muon channel.

7.2. Backgrounds to $Z \to \ell\ell$

Backgrounds to $Z \to \ell\ell$ are very small (1 % or less) relative to the signal. For both the electron and muon channels, contributions from $t\bar{t}$, $Z \to \tau\tau$, and $W \to \ell\nu$ are calculated from simulation, and their associated systematics are calculated as for the signal acceptance times efficiency. For the muon channel, the QCD background is calculated in the same way. For the electron channel, the QCD background is based on the number of events passing the $Z \to ee$ selection in simulation, but with two loose electrons instead of two medium electrons. Then, a measurement in data of the medium-to-loose rejection for electrons from QCD is used to scale this number to the number of expected events where both electrons pass the medium identification requirements.

The predictions of 0.49 ± 0.09 and 0.17 ± 0.01 background events for the electron and muon channels compares favorably with the fact that one same-sign two-electron event and no same-sign muon events are observed passing all of the other Z candidate selection.

8. CROSS SECTION RESULTS

After all of the W event selection, 46 candidate events are observed in the electron channel and 72 are observed in the muon channel. Combining with the integrated luminosity $\int L\,\mathrm{d}t$ of the sample, the acceptance times efficiency $A_W \times C_W$ and the background estimates $N_{\text{background}}$, the cross section can be calculated using the formula

$$\sigma = \frac{N_{\text{cand}} - N_{\text{background}}}{A_W \times C_W \times \int L\,\mathrm{d}t} \ .$$

The W cross section input and results for the electron and muon channels are presented, along with the combined result, in Table III. The uncertainties on the cross sections include the 11% uncertainty on the luminosity [11]. The results are all in agreement with the NNLO standard model prediction of 10.46 ± 0.02 nb, as calculated using the FEWZ program [12, 13] with the MSTW2008 parton distribution functions [14].

The Z cross section inputs and results are shown in Table IV. There are 46 candidate events passing all event selection in the electron channel and 79 in the muon channel. The cross section times branching ratio is calculated using an equivalent formula to the one used for the W result. The predicted cross section times branching ratio for 66 GeV $< M_{\ell\ell} <$ 116 GeV is 0.964 ± 0.039 nb, also calculated in the same way as for the W.

Table IV: Results for the Z cross section times branching ratio to leptons, with inputs.

channel	**int. lum. (nb^{-1})**	N_{cand}	$N_{\text{background}}$	**acceptance x efficiency**	$\sigma\times$ **BR (nb)**
electron	219	46	0.49 ± 0.09	0.288 ± 0.091	0.72 ± 0.11 (stat) ± 0.10 (sys) ± 0.08 (lum)
muon	229	79	0.17 ± 0.01	0.387 ± 0.057	0.89 ± 0.10 (stat) ± 0.07 (sys) ± 0.10 (lum)
combined	-	125	-	-	0.83 ± 0.07 (stat) ± 0.06 (sys) ± 0.09 (lum)

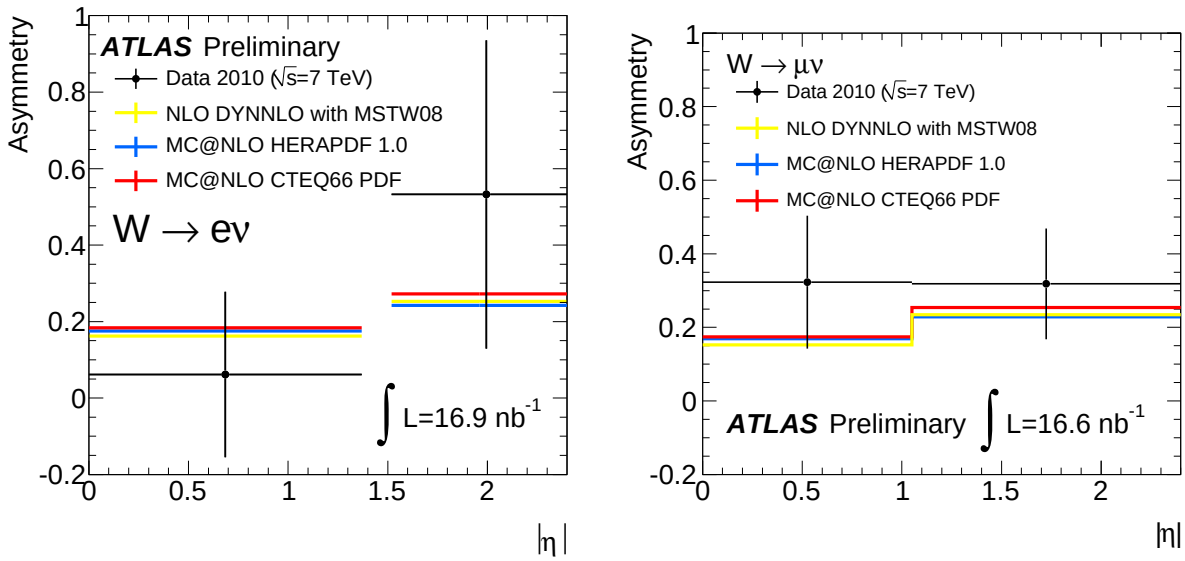

Figure 5: Lepton charge asymmetries in W production as a function of lepton pseudorapidity in the electron (left) and muon (right) channels, compared to three theoretical predictions (see text).

9. W CHARGE ASYMMETRY

One distinctive feature of W production at the LHC is that, because it is a proton-proton collider, more positive than negative Ws are produced. Also, the asymmetry depends on the momentum fraction carried by the colliding quarks and antiquarks, so the ratio of the number of W^+ to the number of W^- produced depends on the lepton pseudorapidity. Using the W sample selected for the cross section measurement, it is possible to measure the charge asymmetry, defined as

$$A = \frac{\sigma^{\ell^+} - \sigma^{\ell^-}}{\sigma^{\ell^+} + \sigma^{\ell^-}} \ ,$$

where $\sigma^{\ell^{+(-)}}$ is the cross section measured with positive (negative) leptons. The fiducial cross sections, defined with A_W set to 1.0, are used to measure the asymmetry, reducing the dependence of the result on theoretical assumptions. The results for the electron and muon channels in two bins of $|\eta|$ are shown in Figure 5. The integral results are 0.21 ± 0.18 (stat.) ±0.01 (sys.) in the electron channel and 0.33 ± 0.12 (stat.) ± 0.01 (sys.) in the muon channel. These may be compared to the NLO theoretical prediction, 0.20, which is calculated using the DYNNLO [15] program with the MSTW08 PDF set [14]. Figure 5 includes that prediction as well as ones from MC@NLO [10] interfaced with the CTEQ6.6 [16] and HERAPDF 1.0 [17] PDF sets.

10. SUMMARY

The distinctive signatures of W and Z production have been observed at the ATLAS detector at the LHC. First cross section measurements have been performed, and the results are in overall good agreement with the Standard Model predictions. Furthermore, the expected charge asymmetry in W production, a unique feature of W production in proton-proton collisions, has been observed and measured. These first measurements will pave the way for a full program of measurements of the W and Z at the LHC, which will deepen our understanding of the Standard Model as well as establishing key tools, such as lepton identification, for use in the detection of rare and new processes.

References

1 UA1 Collaboration, G. Arnison et al., *Experimental observation of isolated large transverse energy electrons with associated missing energy at $\sqrt{s}$ = 540 GeV*, Phys. Lett. **B122** (1983) 103–116.

2 UA2 Collaboration, M. Banner et al., *Observation of single isolated electrons of high transverse momentum in events with missing transverse energy at the CERN $\overline{p}p$ collider*, Phys. Lett. **B122** (1983) 476–485.

3 UA1 Collaboration, G. Arnison et al., *Experimental observation of lepton pairs of invariant mass around 95 GeV/c^2 at the CERN SPS collider*, Phys. Lett. **B126** (1983) 398–410.

4 UA2 Collaboration, P. Bagnaia et al., *Evidence for $Z^o \to e^+ e^-$ at the CERN $\bar{p}p$ collider*, Phys. Lett. **B129** (1983) 130–140.

5 The ATLAS Collaboration, G. Aad et al., *The ATLAS Experiment at the CERN Large Hadron Collider*, JINST **3** (2008) S08003.

6 T. Sjostrand, S. Mrenna, and P. Skands, *PYTHIA 6.4 physics and manual*, JHEP **05** (2006) 026.

7 A. Sherstnev and R. S. Thorne, *Parton Distributions for LO Generators*, Eur. Phys. J. **C55** (2008) 553.

8 The GEANT4 Collaboration, S. Agostinelli et al., *GEANT4: A simulation toolkit*, Nucl. Instrum. Meth. **A506** (2003) 250.

9 The ATLAS Collaboration, G. Aad et al., *Electron and photon reconstruction and identification in ATLAS: expected performance at high energy and results at $\sqrt{s}$ = 900 GeV*, ATLAS conference note: ATLAS-CONF-2010-005.

10 S. Frixione and B. R. Webber, *Matching NLO QCD computations and parton shower simulations*, JHEP **0206** (2002) 29. MC@NLO v3.41 including DY patch.

11 The ATLAS Collaboration, G. Aad et al., *Luminosity Determination Using the ATLAS Detector*, ATLAS conference note: ATLAS-CONF-2010-060.

12 K. Melnikov and F. Petriello, *Electroweak gauge boson production at hadron colliders through O(alpha(s)**2)* Phys. Rev. **D74** (2006) 114017.

13 R. Gavin, Y. Li, F. Petriello *et al.*, "FEWZ 2.0: A code for hadronic Z production at next-to-next-to- leading order," [arXiv:1011.3540 [hep-ph]]

14 A. D. Martin, W. J. Stirling, R. S. Thorne, and G. Watt, *Parton distributions for the LHC*, Eur. Phys. J. **C63** (2009) 189–285.

15 S. Catani and M. Grazzini, *An NNLO subtraction formalism in hadron collisions and its application to Higgs boson production at the LHC*, Phys. Rev. Lett. **98** (2007) 222002, `arXiv:hep-ph/0703012`.

16 P. M. Nadolsky et al., *Implications of CTEQ global analysis for collider observables*, Phys. Rev. **D78** (2008) 013004, `arXiv:0802.0007 [hep-ph]`.

17 The ZEUS and H1 Collaboration, *Combined Measurement and QCD Analysis of the Inclusive e p Scattering Cross Sections at HERA*, JHEP **1001** (2010) 109.